RSC Advances

PAPER

View Article Online
View Journal | View Issue

Cite this: *RSC Adv.*, 2023, **13**, 5496

On the specific heat capacity of HITEC-salt nanocomposites for concentrated solar power applications

Dipti Ranjan Parida and Saptarshi Basu *

High specific heat capacity or C_P of molten salt is crucial for concentrated solar power plants as it will enhance the energy density of thermal energy storage. It can be achieved by doping nanoparticles into molten salts. However, reported results show inconsistency in C_P enhancement (positive and negative). Since the results are based on Differential Scanning Calorimeter (DSC) measurements of small batches (<10 mg), the average C_P obtained from these results may not represent the bulk-C_P of the nanocomposite, which is an important parameter from an application viewpoint. Moreover, the methods of salt-nanoparticle composite production lack industrial scalability. In this work, we examined a potentially scalable method based on mechanical shear mixing. The molten-salt of choice was HITEC due to its lower melting point, while inexpensive alumina and silica nanoparticles were used as dopants. To compare and contrast variability in C_P enhancement, the sample selection was made by random sampling; DSC measurement was performed on small-sized batches (<10 mg), and the T-history method was applied on large-sized batches (20 g). While DSC tests indicated a mean decrease in C_P for alumina (−43%) and an increase in C_P for silica nanocomposite (+15%), T-history tests indicated a mean decrement in the bulk-C_P for both alumina (−49%) and silica nanocomposites (−3%). This anomalous behavior in C_P values was further compared using a nonparametric statistical test, the Mann–Whitney U test, which revealed that the C_P of small-sized batches is statistically different from that of large-sized batches. Given their industrial scale of usage, the C_P of the nanocomposite must be measured using both DSC and T-history methods to ascertain the effect of nanoparticles.

Received 20th November 2022
Accepted 9th February 2023

DOI: 10.1039/d2ra07384f

rsc.li/rsc-advances

1. Introduction

Limited fossil fuel reserves will pose a significant challenge to future electricity demand. This can be evaded by improving alternative renewable electric generation technologies.[1] In this regard, concentrated solar power technology plays an essential role as solar energy is abundant. However, solar energy is intermittent owing to day–night, seasonal, and weather fluctuations, necessitating the installation of thermal energy storage in concentrated solar plants (CSP). This storage generally utilizes molten salt as the storage medium because it is stable at higher temperatures (~600 °C).[2] During the peak available hours, excess solar energy is collected in the storage (in the form of the sensible heat of molten salts) and consumed during off-hours. Nevertheless, both the material and operational costs of the molten salts are very high.[3] In order to deal with this problem, attempts are being made to enhance the energy density of the storage by increasing the specific heat capacity of molten salts.

For the past decade, researchers have focused on improving the C_P of molten salt by doping various nanoparticles (NP), usually <3 wt%.[4,5] creating a nanocomposite or nanofluid (in molten state).[6] This paper uses terms nanofluid (NF) and nanocomposite interchangeably. In 2010, Shin *et al.*[7] studied the effect of silica nanoparticles (1–20 nm) on the eutectic salt of lithium carbonate and potassium carbonate (62 : 38 by molar ratio) for a concentration of 1.5 wt% using a two-step preparation method. They reported 74% and 101% C_P enhancement for two selective test samples coarse and fine powders, respectively, taken from a 200 mg prepared sample. The same authors also reported an enhancement of 124% C_P for fine powder and negligible C_P enhancement for coarse powder[8] despite having the same base salt, nanoparticles, concentration, and preparation method as their previous work. For alumina nanoparticles (~10 nm), Shin and Banerjee[9] reported a 32% C_P enhancement at a heating rate of 20 °C min^{-1} in the DSC test. In contrast, Rizvi *et al.*[10] found a 2.53% C_P enhancement at a heating rate of 10 °C min^{-1} for alumina nanoparticles having an average size of 10.8 nm. In addition, they reported that the specific heat capacity enhancement increases with decreasing heating rate with a maximum of 23.4% for a heating rate of 2 °C min^{-1}. Moreover, an anomalous increase in C_P of the nanofluid is also

Department of Mechanical Engineering, Indian Institute of Science, Bangalore 560012, India. E-mail: sbasu@iisc.ac.in

reported in ref. 11 which strongly depended on the chemical composition of the base carbonate salt mixtures (lithium carbonate and potassium carbonate).

For solar salt (eutectic mixture of 60% $NaNO_3$ and 40% KNO_3), 1 wt% SiO_2 nanoparticle (5 nm) resulted 25% enhancement in C_P[12] while in ref. 13 7 nm SiO_2 nanoparticle show −19.3%, 0.8%, and −1.4% C_P enhancement for 0.5, 1, and 1.5 wt% concentration, respectively. Moreover, the researchers in ref. 13 reported both increment and decrement in C_P for Al_2O_3, TiO_2 nanoparticles. A reduction in C_P for 13 nm Al_2O_3 is also reported in ref. 14. With mechanical dispersion of CuO and TiO_2 nanoparticles using ball milling,[15] reported temperature-dependent C_P curves. One interesting observation in their result was that for 1.5 concentration of CuO nanoparticles the C_P curve crosses the C_P curve of the base salt. For mixed nanoparticles based nanofluid (silica 82–86%, alumina 14–18%, 2–200 nm),[16] a minimum −19% and a maximum of 17.9% C_P enhancement is reported. The same authors[17] also reported a 6.1%, −7.8%, and −3.4% C_P enhancement for the salt KNO_3 using 1 wt% SiO_2, Al_2O_3, and SiO_2–Al_2O_3 NPs, respectively. Similar observations are also reported in ref. 18 and 19 for solar salt with alumina and silica nanoparticles using water-dispersion, and melt-stirring preparation methods, respectively. Moreover, in some recent investigations, we could see the nonlinear temperature dependent C_P for NFs.[20,21] To illustrate the inconsistent C_P enhancement of NFs clearly, some reported literature results are summarized in Table 1.

Though extensive research has been conducted on the C_P of nanofluids for Li–K carbonate salt mixture and solar salt, there has been a limited investigation for HITEC salt (eutectic mixture

Table 1 Anomalous specific heat enhancement reported for binary solar salt by doping with nanoparticles of varying size and concentration

Molten salt	Reference	NPs	Size (nm)	Concentration (wt%)	Temperature (°C)	C_P enhanced%
Solar salt, $NaNO_3$–KNO_3 (60 : 40)	Y. Hu *et al.* (2017)[25]	Al_2O_3	20	0.5	260–400	1.9
				1		5.8
				1.5		7
				2		8.3
	M. Chieruzzi *et al.* (2017)[19]	SiO_2	7	1	255–290	2.5
						−28.1
						2.6
						−2
		Al_2O_3	13	1		2.8
						−7.8
						1.8
						−0.9
	B. Dudda *et al.* (2013)[26]	SiO_2	5	1	250–450	10
			10			13
			30			21
			60			28
	M. Schuller *et al.* (2015)[27]	Al_2O_3	40	0.3	350	20.41
				0.53		24.49
				0.78		30.61
				0.96		23.81
				1.19		14.29
	Chieruzzi *et al.* (2013)[18]	Al_2O_3	13	0.5	250–300	−7.60
				1		5.90
				1.5		−3.50
		SiO_2	7	0.5		−19.30
				1		0.80
				1.5		−1.40
		TiO_2	20	0.5		−15.60
				1		−6.30
				1.5		−11.80
	Andreu-Cabedo *et al.* (2014)[28]	SiO_2	12	0.5	250–420	3.41
				1		25.03
				1.5		2.00
				2		3.69
	M. Lasfargues *et al.* (2015)[29]	CuO	29	0.1	440	10.48
				0.5		9.18
				1		8.49
				1.5		2.19
		TiO_2	34	0.1		1.57
				0.5		4.95
				1		4.72
				1.5		4.85

of KnO_3–$NaNO_2$–$NaNO_3$). However, HITEC salt shows better thermophysical properties than other salts and is one of the prime candidates for CSP as heat storage media.[22] In 2014, M. X. Ho *et al.*[23] observed both −1.7% and 7.8% enhanced C_P for 0.5 wt% concentration, and −2.8% and 6.5% enhanced C_P for 1 wt% concentration from HITEC based NF with alumina nanoparticles using a melt-stirring preparation method. In another investigation,[24] the authors reported a 30% enhanced heat capacity for the HITEC salt using Sn/Si_x core–shell nanoparticles at the melting point of the NPs. However, the C_P curves of all HITEC-Sn/Si_x NFs (as shown in ref. 24) are below the base salt's C_P curve (except at the melting point of the NPs) indicating a decrease in heat capacity.

To summarize previous literature, the salt nanocomposite can be synthesized by either wet-dispersion (2-step method) or dry-dispersion (1-step method). The wet-dispersion process can be classified as: (i) water dispersion method (dissolution of salt in water → ultrasonication (100–200 minutes) → drying), (ii) melt-stirring method (nanoparticle addition to molten salt → mechanical stirring → drying) whereas the dry-dispersion process includes (i) ball mill mixing, (ii) mechanical shear mixing. Although nearly all research utilized the 2-step method for salt-nanocomposite preparation, it is very time-consuming, laborious, and unsuitable for industrial production. In contrast, the effect of the 1-step preparation method is rarely studied.[30,31] In almost all literature, the prepared nanocomposite sample size was 200 mg, out of which test samples (∼10 mg) are taken for C_P measurements using DSC. Therefore, the results that were obtained from the test samples are limited by sampling size ratio $\left(\frac{\text{test sample}}{\text{prepared sample}} = \frac{1}{20}\right)$, *i.e.* random sampling is limited, and thus the data variability obtained from these results may not represent for the C_P of bulk nanocomposite. As mentioned in Zhang Yingping *et al.*,[32] the thermophysical properties of these samples are not always similar to that of bulk materials. So, it is not confirmed whether such specific heat enhancement effect will be present in the practical systems.

Moreover, we see both increment and decrement in C_P for molten salt nanocomposites consisting of same base salt, nanoparticle, concentration, and same measurement procedure, as in ref. 19, and varying C_P for selective nanocomposite samples, as in ref. 8 for coarse and fine powder samples. Since we know that the C_P enhancement depends strongly on the concentration of nanoparticle[33] in the base salt, it is not certain whether the test samples collected from the same prepared samples consist of the same concentration (*i.e.*, the drying process may have altered the NP concentration with respect to varying location due to convection current) and hence the irregular C_P enhancements. So, from the perspective of engineering application, a comparative study for the specific heat capacity of molten-salt nanocomposites is needed to capture possible C_P variations by random sampling, and to inquire about its bulk-specific heat capacity with respect to DSC results.

Hence, in this study, HITEC salt nanocomposite is synthesized by the dry-dispersion method using high shear mechanical powder mixture for two different nanoparticles, silica (SiO_2) and alumina (Al_2O_3). The concentration of the nanofluid samples is kept at 1 wt%. Differential scanning calorimetry and T-history methods are used for specific heat measurement of small and large nanofluid samples, respectively. Finally, the resulting nanocomposites are examined for possible microstructures.

2. Experiments

2.1 Materials

HITEC salt (53% KnO_3 + 40% $NaNO_2$ + 7% $NaNO_3$) is used as the base molten salt because its melting point is relatively lower (142 °C), and it is stable at high temperature and less corrosive. The powdered salt was procured from Indrajit Industries (Bangalore, Karnataka, India). Regarding purity, the acceptable level of impurities (as provided by the manufacturer) were 0.025% sulfur and 0.1% chloride. The thermophysical properties of pure HITEC salt, as quoted by the manufacturer, are given in Table 2.

Two nanoparticles chosen for this study were silica (SiO_2) and alumina (Al_2O_3) (Sigma-Aldrich Product no: 637238 and 544833). The corresponding nanoparticle size for silica and alumina are 10–20 nm and <50 nm, respectively. The TEM image of Al_2O_3 nanoparticle indicates that the alumina nanoparticles are of rod type (same as ref. 34). Whereas the TEM image of SiO_2 shows that the shape of the silica nanoparticles is nearly spheroid (see Fig. 1b). The physical properties corresponding to the nanoparticles are shown in Table 3.

2.2 Nanocomposite synthesis

Fig. 2 shows the schematic of the 1-step dry dispersion method for nanocomposite preparation. For this experiment, the nanoparticle (SiO_2/Al_2O_3) concentration in the base salt is chosen to be 1 wt%. First, both HITEC salt and nanoparticles are desiccated at 120 °C for 3 hours. Then measured in a microbalance (A&D GR-202, ±0.01 mg). The salt-nanopowder composite is prepared in an in-house-developed laboratory powder mixture (high shear mixer: 4-blade design, 550 watts, and 18 000 rpm). In total, 150 grams of nanocomposite (salt = 148.5 g, nanoparticle = 1.5 g) is prepared for each nanoparticle powder so that three samples of 20 grams each can be drawn for the T-history experiment. Since the sample size requirement for

Table 2 Thermophysical properties of pure HITEC salt

Properties	Value
Melting point	142 °C
Thermal decomposition	>600 °C
Viscosity	1.1×10^{-6} m^2 s^{-1} at 400 °C
Specific gravity	1.94 at 200 °C
	1.81 at 400 °C
	1.78 at 500 °C
pH	6.5–8.5
Thermal conductivity	$0.605 \frac{\text{W}}{\text{m °C}}$ (240–365 °C)
Liquid specific heat capacity	0.34 kcal kg^{-1} °C^{-1}

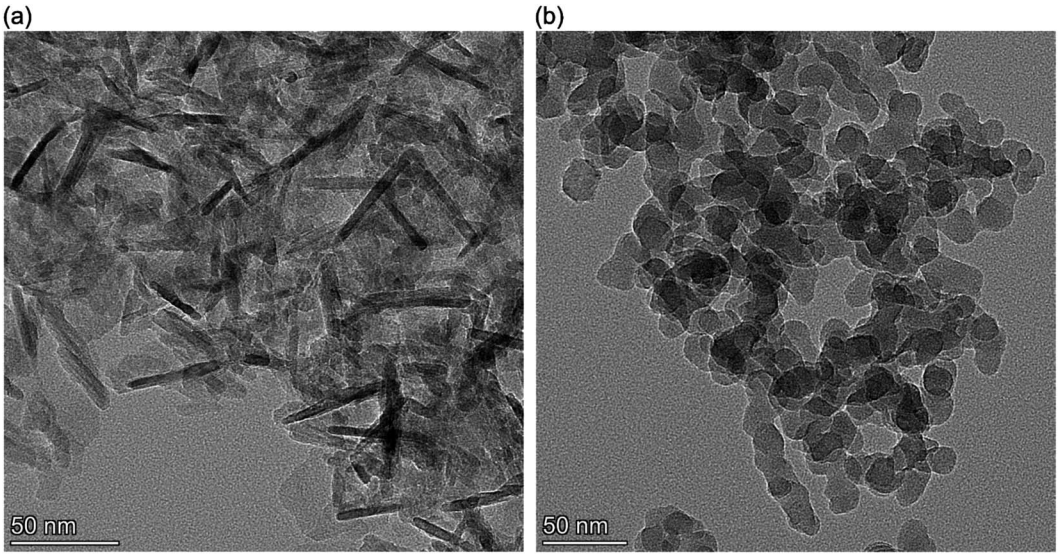

Fig. 1 TEM images of nanoparticles; (a) rod-type alumina; (b) spheroid shaped silica.

Table 3 Properties of nanoparticles

Nanoparticle	Size (nm)	Density (g mL^{-1})	Surface area (m^2 g^{-1})	Purity
Al_2O_3	<50[a]	3.97[b36]	35–43[b36]	98%[a]
SiO_2	10–20[a]	2.2–2.6[a]	63.4 ± 0.8[b35]	99.5%[a]

[a] Mentioned in the product catalog. [b] Results reported in the literature for the same product.

the DSC is in milligrams, 150 grams of nanocomposite is sufficient for this random sampling, which is intended to capture any variability in the nanocomposite if present.

2.3 Specific heat capacity measurement

2.3.1 Differential scanning calorimetry. To determine the C_P of HITEC salt and the nanocomposites, a differential scanning calorimetry test is performed on a Mettler Toledo DSC instrument (Mettler-Toledo DSC-832[e] calorimeter). Initially, the stored desiccated samples are heated to 120 °C for 1 hour prior to the measurement. A microbalance (ESSAE, VIBRA model-HTR 220 E, 0.0001 g) is used for all sample mass measurements (≤10 mg), and hermetically sealed standard Aluminum crucibles (40 μl) are used for the DSC experiment. To ensure proper contact with the bottom of the crucible, the nanocomposite powder mixture is compacted with a Teflon rod.

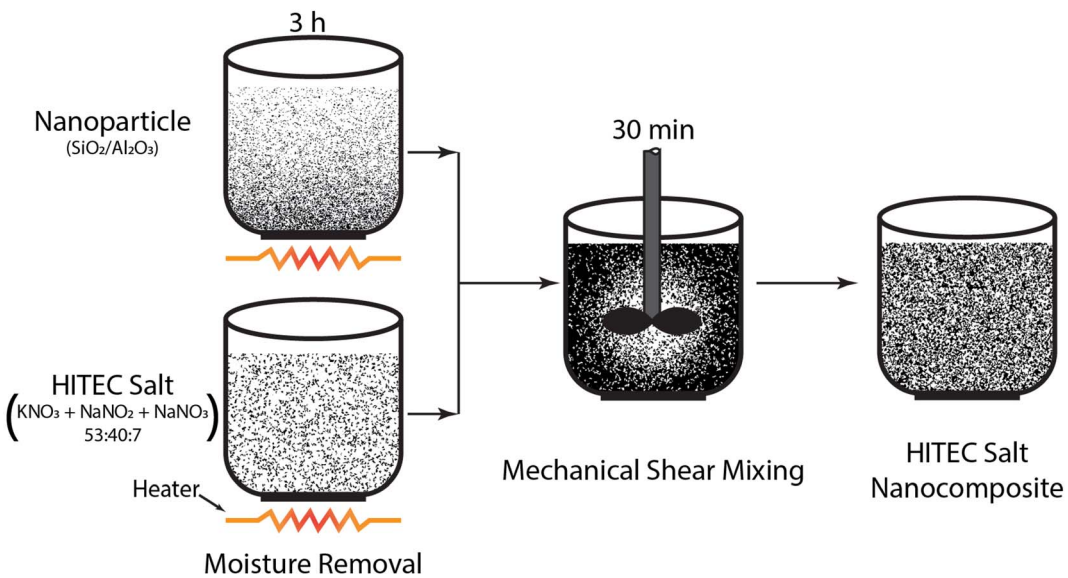

Fig. 2 Schematic showing the single-step preparation (dry dispersion) of salt-nanopowder composite using mechanical shear mixing. Nanoparticle and HITEC salt are separately heated for 3 hours for moisture removal and then shear mixed for 30 minutes. The resulting nanocomposites are then stored in a desiccator for further use.

Moreover, blank correction is confirmed before sample measurements.

The specific heat capacity of all samples is determined by the direct method;[37]

$$C_P = \frac{HF}{m\beta} \quad (1)$$

where C_P is the specific heat capacity of the sample (J g^{-1} °C^{-1}), HF is the heat inflow rate (mW) obtained by the subtraction of the blank curve from the DSC signal, β is the heating rate (°C s^{-1}), and m is the sample mass (mg). The heating rate (β) of 20 °C min^{-1} is chosen in accordance with ASTM standard E1269-11.[38] Firstly, the procured HITEC salt sample was verified with respect to the manufacturer's data and with literature. Then test runs were carried out for nanocomposite samples, and the liquid average C_P are reported for comparison.

2.3.2 T-History method. The C_P of bulk materials is determined by using the T-history method.[32] Schematic of the experimental setup is shown in Fig. 3, in which both reference sample (pure HITEC salt) and test samples (salt nanocomposites; alumina NF, and silica NF) are kept inside a heat-controlled environment, whose temperature is fixed. The sample holders used in this experiment were borosilicate glass tubes with an inner diameter of 21 mm, an outer diameter of 25 mm, and a height of 95 mm. The temperature–time curve of all samples (20 g), including the environment, are recorded using K-type thermocouples (HEATCON Instruments Pvt. Ltd., Bangalore, India) and NI (National Instruments) data acquisition system. The surrounding air temperature is the average of two thermocouples (T_a1 and T_a2) readings.

Since the T-history experiment involves dynamic temperature measurement, *a priori* of the thermal analysis, the following points are checked; (1) cross-sectional thermal gradient in the surrounding atmosphere, (2) time constant of the thermocouple. In the present experiment, a maximum gradient of ±0.285 °C cm^{-1} along the length and ±0.133 °C cm^{-1} along the width of the chamber are noticed. Accordingly, the samples are kept side by side along the width. Moreover, a time constant of ~200 ms is quoted by the supplier for the K-type thermocouple (uncoated, diameter = 1.5 mm). As it is general practice to keep a time gap for sampling higher than that of time constant, we have recorded the thermocouple readings at 1.1 second intervals.

For the thermal analysis, firstly, the temperature of the surrounding air is ramped from room temperature to 170 °C and kept for 0.5 hours to ensure the complete melting of HITEC salt. Then the chamber temperature is again improved to 450 °C with a rate of 10 °C min^{-1}. A dwell time of 2 hours is given so that all samples and the ambient come into equilibrium. Finally, the heaters are switched off, and the cooling temperature history (cooling curve) is recorded. This experiment is repeated three times for three different batches of nanocomposite (alumina NF and silica NF), and their results between 200–400 °C are reported accordingly.

The primary assumption in using the T-history method is to satisfy the lumped capacitance of sample materials, *i.e.*, the Biot number, $\mathrm{Bi}\left(\frac{hR}{2k}\right) < 0.1$,[32,39] where Bi is the Biot number, h is the heat transfer coefficient of the surrounding air, R is the outer radius of the sample holder, and k is the thermal conductivity of

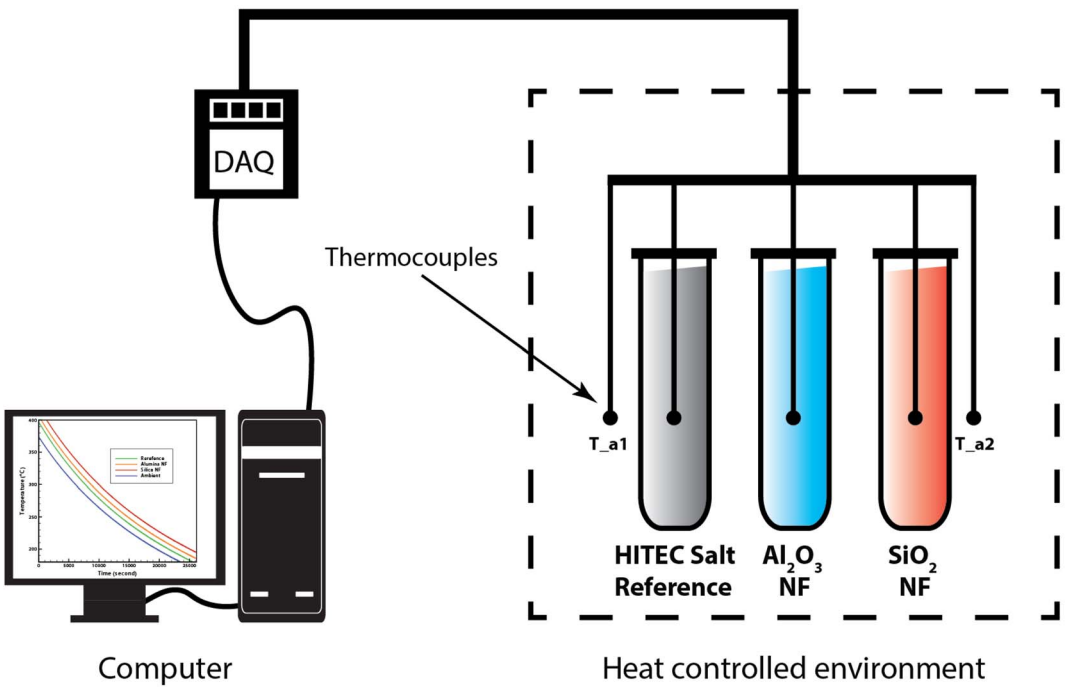

Fig. 3 Schematic of temperature history (T-history) experimental setup. Samples are melted in borosilicate tubes at 500 °C and then allowed to cool. Three thermocouples are used to measure the cooling curve of the samples. T_a1 and T_a2 are thermocouples used to measure the mean surrounding air temperature. DAQ is the data acquisition system for temperature logging.

the samples. For a laminar natural convection, h usually lies below $2\frac{\mathrm{W}}{\mathrm{m}^2\ ^\circ\mathrm{C}}$.[40,41] So, the Biot number for the pure HITEC salt ($\sim$0.021) satisfies the criterion. Moreover, the thermal conductivity of the HITEC salt increases when doped with nanoparticles.[42] Hence the Biot number of nanofluids will be smaller than that of pure salt and will be content with the lumped capacitance assumption.

At any instant of time, the amount of heat released by the samples to the surrounding air can be written as;

$$mC_{\mathrm{P}}\frac{\partial T}{\partial t} = hA_{\mathrm{C}}(T_{\mathrm{air}} - T) \quad (2)$$

where m denotes the mass of the samples (g), C_{P} denotes the specific heat capacity (J g^{-1} °C^{-1}), $\frac{\partial T}{\partial t}$ denotes the slope of the cooling curve (°C s^{-1}), h denotes the convective heat transfer coefficient of surrounding air $\left(\frac{\mathrm{W}}{\mathrm{m}^2\ ^\circ\mathrm{C}}\right)$, and A_{C} denotes the characteristic area for convection. In this experiment, the heat conduction from the bottom surface of the sample holder is avoided by keeping an insulation layer (50 mm glass wool insulation) between the tube and the heating chamber during the cooling process. Thus A_{C} represents the cylindrical surface of the tubes. Moreover, T and T_{air} denote the instantaneous temperatures of the sample and the surrounding air (°C), respectively. Since both m, and A_{C} are constant for all samples, assuming negligible variation in h, the ratio of specific heat capacity at any fixed temperature can be found from :[43]

$$\frac{C_{\mathrm{P_{nano}}}}{C_{\mathrm{P_{salt}}}} = \frac{\left(\frac{\partial T_{\mathrm{s}}}{\partial t}\right)_{\mathrm{salt}}}{\left(\frac{\partial T_{\mathrm{s}}}{\partial t}\right)_{\mathrm{nano}}}\frac{(T_{\mathrm{air}} - T_{\mathrm{s}})_{\mathrm{nano}}}{(T_{\mathrm{air}} - T_{\mathrm{s}})_{\mathrm{salt}}} \quad \text{at any fixed sample temperature } T_{\mathrm{s}} \quad (3)$$

where the subscripts salt, and nano refer to pure HITEC salt and nanofluid (alumina/silica), respectively. For a detailed discussion on the T-history method and its calculations, see ref. 43–45. In the end, the surface morphology of the nanocomposites is investigated for possible representative microstructures using scanning electron microscopy (SEM; make: Carl Zeiss Ultra 55 field-emission scanning electron microscope) with an accelerating voltage of 5 kV at the Micro and Nano Characterization Facility (MNCF), Centre for Nano Science and Engineering, IISc Bangalore.

3. Results and discussion

The melting point and the specific heat capacity (C_{P}) of the procured HITEC salt are verified using differential scanning calorimetry. The DSC curve of the pure salt is shown in Fig. 4. It is seen that the melting peak of HITEC salt starts at around 142 °C and ends at 162 °C. Moreover, the specific heat capacity at the liquid phase is weakly dependent on the temperature having an average value of 1.42347 J g^{-1} °C^{-1}. It is important to note that the upper bound of the C_{P} for HITEC salt is reported to be 1.56 J g^{-1} °C^{-1} in previous literature.[46,47] However, average C_{P} of the present study is found to be in good agreement with the literature ref. 48 ($C_{\mathrm{P}} = 1.424$ J g^{-1} °C^{-1}), ref. 23 ($C_{\mathrm{P}} = 1.37$–1.48 J g^{-1} °C^{-1}), ref. 49 ($C_{\mathrm{P}} = 1.439$ J g^{-1} °C^{-1}), and ref. 50 ($C_{\mathrm{P}} = 1.40$ J g^{-1} °C^{-1}) as well as with the value cited by the manufacturer (0.34 kcal kg^{-1} °C^{-1}).

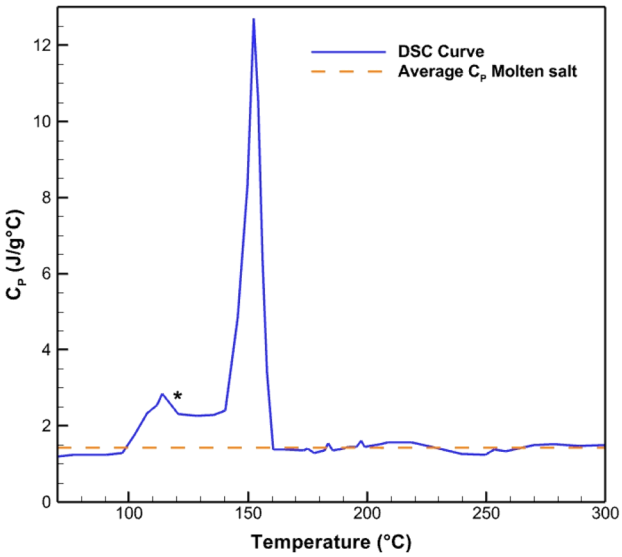

Fig. 4 C_{P} curve of HITEC salt obtained from DSC measurement. The melting point is found to be 142 °C (beginning of melting peak). The average specific heat capacity of 1.42347 J g^{-1} °C^{-1} is obtained from the curve in the liquid phase. The minor peak (highlighted as *) is caused by solid transformation, as reported in previous literature.[51,52]

The results obtained from the DSC measurements (C_{P} *vs.* T curves) of alumina and silica nanofluids are shown in Fig. 5, which reveals two interesting features. Firstly, the C_{P} of both nanofluids are temperature dependent. Secondly, there is a decrease in C_{P} with respect to the base molten salt ($C_{\mathrm{P}} =$ 1.42347 J g^{-1} °C^{-1}) for Al_2O_3 NF for all three batches (#1 to #3), and an increase in C_{P} for SiO_2 NF (batch #1 and #2). However, there is a decrease in C_{P} for the batch #3 of SiO_2 NF. Regarding the mean specific heat capacity of nanofluids, a sampling interval of 10 °C gives 0.810684 $\pm$ 0.1138 for alumina NF, and 1.634839 $\pm$ 0.204117 for silica NF. In consequence, the enhancement in C_{P} of HITEC salt owing to the doping of 1% nanoparticle can be presumed to be −43.0487%, and 14.84886% for alumina and silica nanofluids, respectively. In addition, the theoretical C_{P} of the NFs can be calculated from the mixing theory:

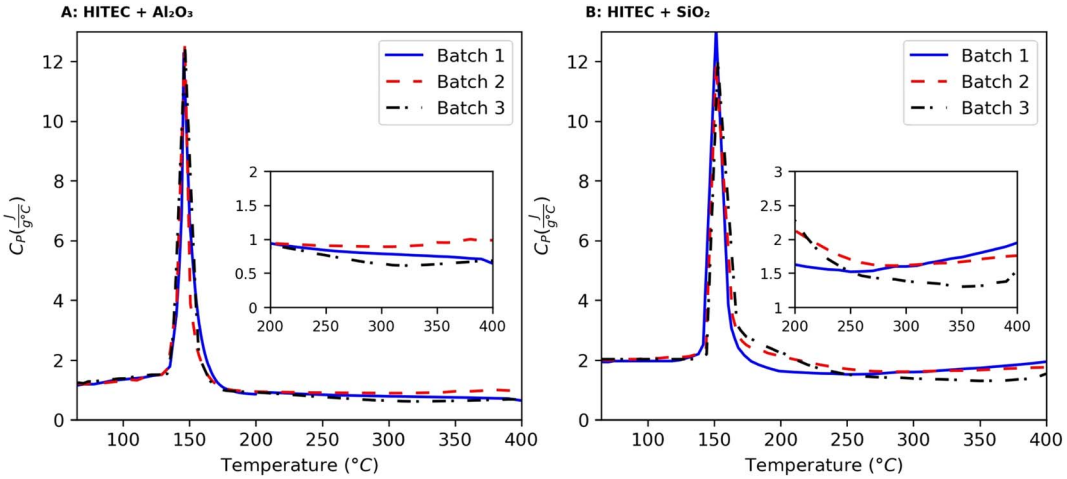

Fig. 5 DSC plot of HITEC-salt nanocomposites (1% wt. fraction) shown between 200 and 400 °C at a sweep rate of 20 °C min^{-1}; (A) alumina nanofluid, (B) silica nanofluid. Each plot consists of measurements using 3 batches (batch 1–3).

$$C_{P(NF)} = \frac{m_{np} C_{P_{np}} + m_{salt} C_{P_{salt}}}{m_{np} + m_{salt}} \quad (4)$$

to be $C_{P(Al_2O_3\text{-NF})} = 1.416965$, and $C_{P(SiO_2\text{-NF})} = 1.416235$; each is having a decrement in C_P ~0.5%. So, it is clear from the discussion that this anomalous C_P in molten salt nanofluid deals with some microscopic phenomenon that is temperature-dependent and certainly cannot be explained by classical heat transfer considerations.

In the present work, therefore, the T-history method is used to investigate whether such microscopic phenomena have any profound effect on the bulk-specific heat capacity of the nanofluids. The results obtained from this temperature history experiment are shown in Fig. 6a–c, where the test samples are cooled inside the static-air chamber, as described in Section 2.3.2. The primary observation of these cooling curves reveals that both Al_2O_3 and SiO_2 nanofluids cool faster than base HITEC salt in test #1, and #2; however, the cooling curve in the SiO_2 NF for the test #3 is slower compared to the base salt indicating an increase in specific heat capacity. On reverting to the previous discussion of DSC results, a similar variation is observed in SiO_2 NF, where sample #3 diverges from samples #1 and #2. These results are not surprising as both increment and decrement of C_P of nanofluids are already reported in earlier studies[18,19] using DSC. The critical point, however, to note here is that we still see such irregular C_P behavior in the bulk samples.

Regarding quantitative estimation, the C_P ratios of the nanocomposites $\left(\frac{C_{P_{nano}}}{C_{P_{salt}}}\right)$ are calculated from the cooling curves using eqn (3) at 10 °C intervals and are shown in Fig. 6d–f. On average, the bulk-specific heat capacity of the nanofluids is 0.729959 ± 0.176598 for alumina NF and 1.383344 ± 0.426798 for silica NF. In consequence, a decrement in C_P of HITEC salt owing to the doping of 1% nanoparticle can be found to be −48.7198% and −2.81887% for alumina and silica nanofluids, respectively. While average C_P values of the alumina NFs as obtained from both DSC and T-history methods are comparable, the outcomes for silica NFs are quite different. The minimum and maximum enhancement in C_P of silica-NF are −9% and 60% from DSC, and −38% and 42% from T-history tests. Thus, it indicates that the result obtained from small samples using DSC may not represent the bulk behavior/C_P of the NFs. In addition, Fig. 6d–f shows that the C_P ratios of all nanofluid samples are nearly linear with respect to temperature and are approaching a unit value (*i.e.*, $\frac{C_{P_{nano}}}{C_{P_{salt}}} = 1$; specific heat capacity of the base molten salt). This observation, however, is consistent with Ho an Pan,[23] in which the C_P curves of nanocomposites at different concentrations approaches the base salt with increase in temperature. So, it signifies that the microscopic phenomena which are contributing to an increment/decrement of C_P of the nanofluid are quasi-stable. Rapid agglomeration and sedimentation of nanoparticles may be responsible for this instability owing to the decrease in density of the base molten salt (specific gravity: from 1.94 at 200 °C to 1.81 at 400 °C) with rising temperature.

For a concise comparison between DSC and T-history experimental results, the C_P increment/decrement percentage of both nanocomposites are shown in a Box-and-Whisker plot with data overlay (Fig. 7). Upon closer inspection, it reveals that the results of both tests are not completely different but rather show different central measures and variability in one test compared to the other as:

- For Al_2O_3 nanoparticle-based composite, both tests show a decrement in C_P.
- For SiO_2 nanoparticle-based composite, both tests show increment and decrement in C_P.
- The interquartile ranges of the results obtained in both tests overlap for Al_2O_3 and SiO_2 nanocomposites.

However, there are differences in their statistical moments (mean and median). From these statistical moments, we deduce the central tendency/measure of the samples. For this study, the central measures of the tests are not comparable as:

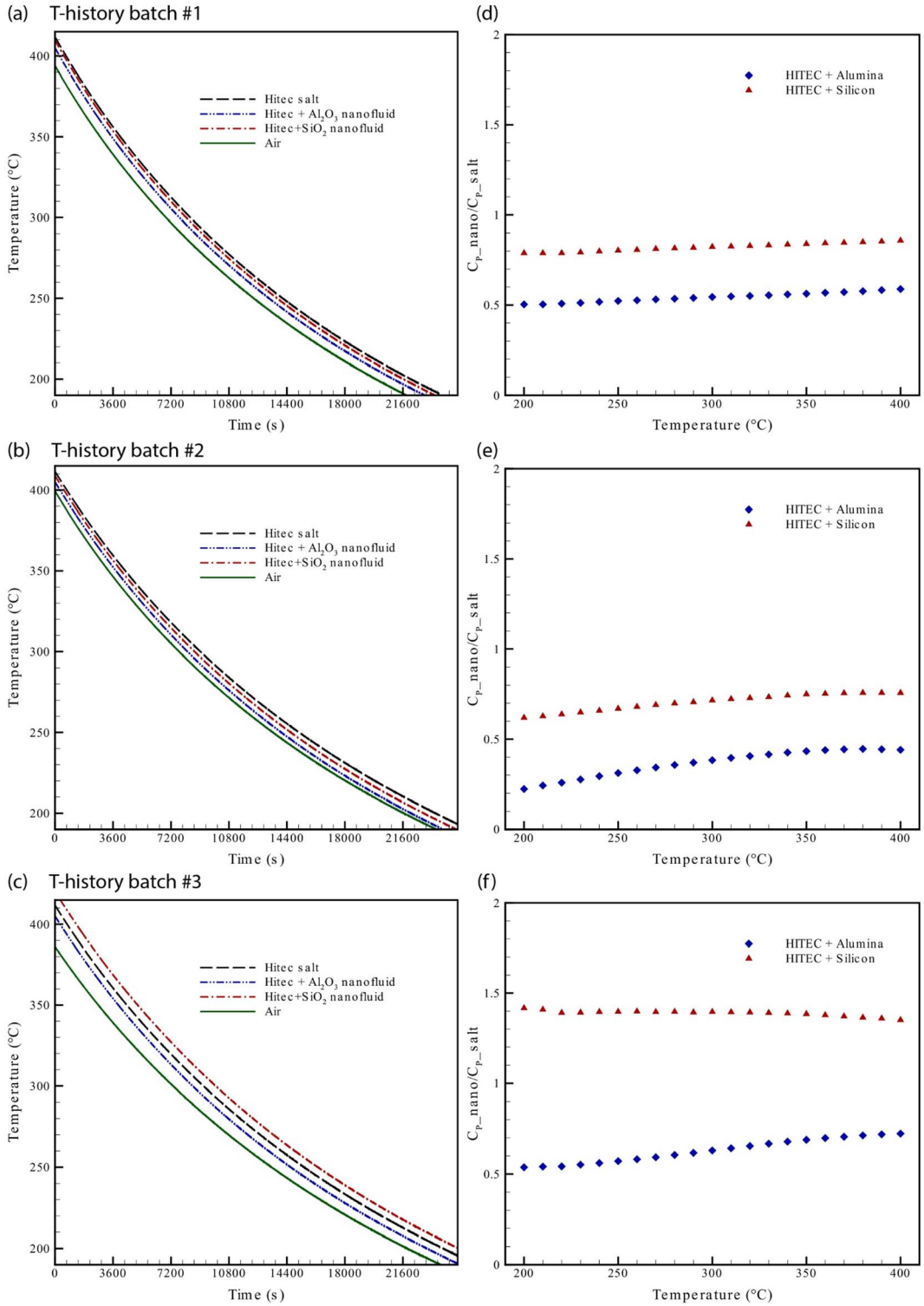

Fig. 6 Results obtained from three T-history tests for all samples shown between 200 and 400 °C; (a)–(c) are the cooling curves (temperature *vs.* time curve) for different batches; (d)–(f) are the corresponding ratio of specific heat capacity of nanofluids with respect to the reference sample (pure HITEC salt).

• Although the interquartile ranges overlap, the medians of the T-history results are lower than that of the DSC results for both nanofluids.

• Both T-history mean and median values of SiO_2 nanofluid are of opposite sign to that of the DSC experiment.

• A wider interquartile range for SiO_2 NF results obtained from the T-hisory test indicates a larger variability of bulk C_P.

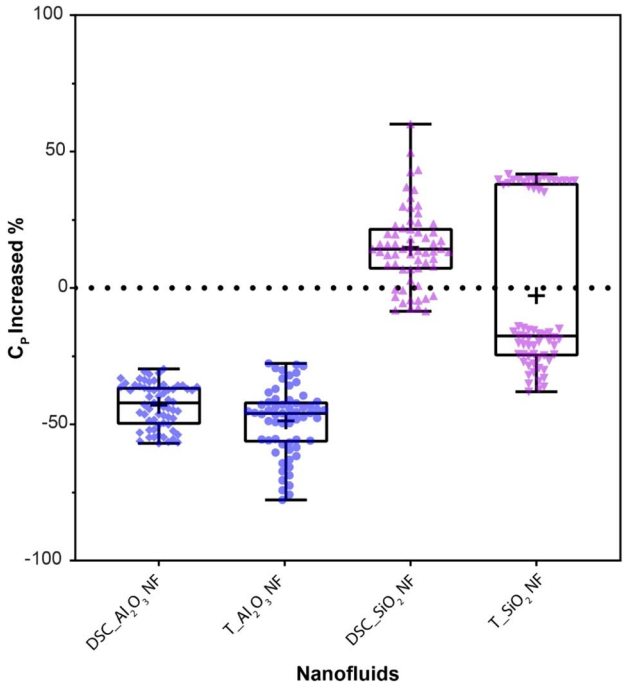

Fig. 7 Box-and-whisker plot with data overlay for specific heat capacity enhanced percentage $\left(\frac{C_{P_{nano}} - C_{P_{salt}}}{C_{P_{salt}}} \times 100\right)$ of HITEC-salt nanocomposites corresponding to both DSC and T-history tests; light blue-alumina nanofluid; light purple-silica nanofluid; +, mean value.

This indicates that the resultant effect on C_P of salt nanocomposite for larger weight samples (bulk-C_P) can be different than it seems from the smaller samples. There are two potential reasons for such behavior. Firstly, the agglomerative scale of nanoparticles can vary in large-size samples, and there is a possibility that we may not be able to capture these in small-size samples. Secondly, there is a possibility of a difference in the nanoparticle distribution in both samples, and we only capture a subset of the overall distribution in the DSC test.

Considering all the above analysis, we now ask an interesting question: are the results obtained from both DSC and T-history experiments from the same population? In an attempt to answer this question, we have performed a nonparametric Mann–Whitney U test.[53,54] It is a well-known statistical test for comparing two sample groups where the null hypothesis is H_0: both sample groups are the subsets of the same population. In this test, the U-test static is the minimum U_i, which is obtained by

$$U_i = n_1 n_2 + \frac{n_i(n_i+1)}{2} - \sum R_i \; ; \quad i = 1, \text{ and } 2 \tag{5}$$

where U_i, and n_i are the U-static, and the number of values from the sample of interest, respectively. $\sum R_i$ is the sum of the ranks from sampe of interest. The characteristic z-score (z^*) is also calculated by

$$z^* = \frac{U - \overline{x_U}}{S_U} \tag{6}$$

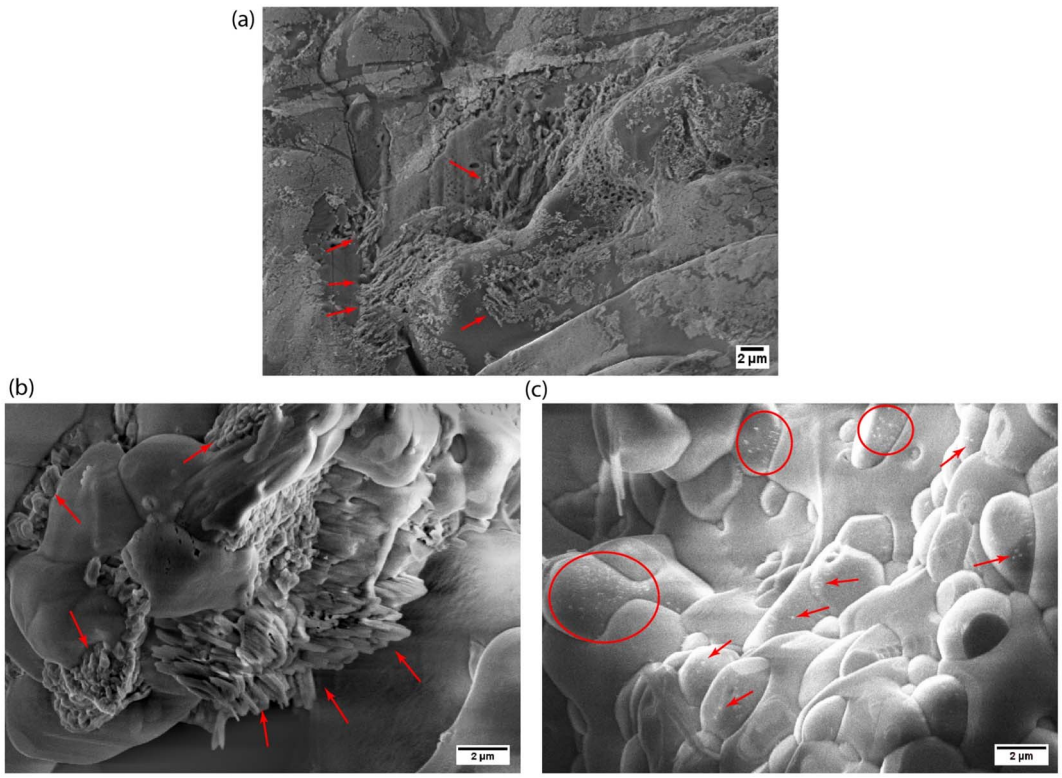

Fig. 8 Representative microstructures of HITEC salt nanocomposites after T-history experiments; (a) aggregated network structure found in alumina nanocomposite, (b) aggregated network structure found in silica nanocomposite, (c) isolated particle structure found in silica nanocomposite.

where $\overline{x_U}$, and S_U are the mean and standard deviation obtained by $\overline{x_U} = \frac{n_1 n_2}{2}$, and $S_U = \sqrt{\frac{n_1 n_2 (n_1 + n_2 + 1)}{2}}$, respectively. In order to test the null hypothesis, this z^* is then compared to a critical threshold obtained from a standard normal distribution for a fixed confidence level. For the details of this method, the readers may refer to the book.[55] The z^* obtained for alumina and silica nanofluids are −2.505, and −3.656, respectively. Since the critical threshold of z-score for 95% confidence is ±1.96, z^* lies outside of this interval, and we reject the null (H_0) in both tests with the inference that the results obtained from DSC and T-history experiments aren't from the same population. The point of this discussion is that the bulk-specific heat capacity values are statistically different than that of the specific heat capacity values obtained from the DSC test (certainly for this 1-step dry dispersion preparation method).

From a microstructure point of view, we have characterized the nanofluid samples obtained from the T-history experiment using scanning electron microscopy (SEM). The representative microstructures of both Al_2O_3 and SiO_2 nanocomposites are shown in Fig. 8. Based on the observation, the obtained microstructures can be classified into two types: (i) aggregated network structure, as seen in Fig. 8a and b, and (ii) isolated particle structure, as seen in Fig. 8c. Similar network-like microstructures were observed earlier in ref. 56 and 57 and an isolated-particle structure was reported in ref. 23. We presume that the aggregated network structures are semisolid layers and are responsible for a decrease in C_P whereas the isolated particle structures favor C_P enhancement. Moreover, the percentage of these microstructures may vary with in a nanocomposite batch owing to the variations in nanoparticle dispersion which further depend on the preparation method and agglomeration of nanoparticles. Furthermore, we believe the rod type Al_2O_3 nanoparticles are favorable to form network structures, and hence we see a decreased C_P in DSC and T-history experiments. However, spheroid shape of SiO_2 nanoparticles forms both type of structures and depending on their percentage we see either an enhancement or diminution of C_P. In the view of above analysis, it can be concluded that there is an agglomerative-scale dependency on the bulk C_P of molten salt nanocomposites.

4. Conclusion

The current article reports on the specific heat capacity (C_P) of HITEC salt nanocomposites prepared by 1-step dry dispersion method using mechanical shear mixing. In which alumina and silica nanoparticles with distinct morphological features (Al_2O_3: rod type, <50 nm; SiO_2: spheroid type, 10–20 nm) were doped into the base salt at 1 wt% concentration. The C_P measurements were carried out using DSC and T-history test methods for small (≤10 mg), and large (20 g) random samples, respectively, aiming to determine whether or not the specific heat capacity measured in DSC is representative of the bulk specific heat capacity of the nanocomposite. The key findings of the study can be summarized as follows.

1. The rod type Al_2O_3 nanoparticle results in a decrement in C_P of the HITEC salt, about −43% from the DSC, and −49% from the T-history experiment.

2. The spheroid type SiO_2 nanoparticle results in both increments and decrements in C_P for silica nanocomposite as obtained from DSC and T-history tests. The minimum and maximum C_P enhancement in silica-NF are found to be −9% and 60% from DSC, and −38% and 42% from T-history tests, respectively. However, the average C_P enhancement percentages are of opposite sign (+15% for DSC test and −3% for T-history test), which indicates that the C_P result of DSC test is not representative of the bulk C_P that obtained from T-history test.

3. More importantly, from the statistical analysis (Mann–Whitney U test with 95% confidence interval), it is inferred that the parent nanocomposite samples/statistical population of the DSC and the T-history test batches are unalike. Since the test batches are taken randomly from the same original sample, it is believed that there is an inhomogeneity in nanoparticle dispersion within the prepared nanocomposite sample; which explains why diverging C_P increment/decrement is observed for selective nanocomposite samples within the same prepared sample, even in studies by other groups reporting 2-step preparation method.

4. From microscopic characterization, only aggregated-network microstructure is found for Al_2O_3 nanocomposite, whereas both network and isolated-particle type microstructures are found in SiO_2 nanocomposite. It is believed that the bulk C_P of the silica NF in the T-history experiment differs from the DSC test due to a non-uniform distribution of these representative microstructures in the large samples, which depends on the preparation procedure and stability of nanoparticles.

Based on the presented results, there is a possibility that the behavior of C_P obtained from DSC may differ from the bulk-specific heat capacity substantially. To conclude whether the prepared nanocomposite has indeed achieved C_P enhancement, both DSC and T-history methods must be used in a complementary manner.

Author contributions

Dipti Ranjan Parida: conceptualization, investigation, data curation, formal analysis, writing – original draft. Saptarshi Basu: conceptualization, project administration, supervision, writing – review & editing.

Conflicts of interest

There are no conflicts to declare.

Nomenclature

ASTM	American Society for Testing and Materials
β	Heating rate (°C s^{-1})
C_P	Specific heat capacity (J g^{-1} °C^{-1})
CSP	Concentrated solar power
DSC	Differential scanning calorimeter

HF	Heat inflow rate (mW)
H_0	Null hypothesis
m	Mass of the sample (mg)
n	Number of values in a sample group
NF	Nanofluid
NP	Nanoparticle
R_i	Individual rank of sample values
S_U	Representative standard deviation in Mann–Whitney U test
SEM	Scanning electron microscope
TEM	Transmission electron microscope
T_s	Sample temperature (°C)
$\frac{\partial T_s}{\partial t}$	Slope of the colling curve (°C s^{-1})
U	U-static in Mann–Whitney U test
$\overline{x_U}$	Representative mean in Mann–Whitney U test
z^*	Characteristic z-score in Mann–Whitney U test

Acknowledgements

The present study is supported by the Ministry of human resource development and the Ministry of New and Renewable Energy, Govt. of India, under the IMPRINT initiative (grant number/Project no: 4424).

References

1 P. A. Owusu and S. Asumadu-Sarkodie, A review of renewable energy sources, sustainability issues and climate change mitigation, *Cogent Engineering*, 2016, **3**(1), DOI: **10.1080/23311916.2016.1167990**.

2 E. González-Roubaud, D. Pérez-Osorio and C. Prieto, Review of commercial thermal energy storage in concentrated solar power plants: steam *vs.* molten salts, *Renewable Sustainable Energy Rev.*, 2017, **80**, 133–148, DOI: **10.1016/j.rser.2017.05.084**.

3 C. S. Turchi, J. Vidal and M. Bauer, Molten salt power towers operating at 600–650 °C: salt selection and cost benefits, *Sol. Energy*, 2018, **164**, 38–46, DOI: **10.1016/j.solener.2018.01.063**.

4 H. E. Kwak, D. Shin and D. Banerjee, Enhanced Sensible Heat Capacity of Molten Salt and Conventional Heat Transfer Fluid Based Nanofluid for Solar Thermal Energy Storage Application, *ASME 2010 4th Int. Conf. Energy Sustain. ES*, 2010, vol. 2, pp. 735–739, DOI: **10.1115/ES2010-90295**.

5 D. Shin, B. Jo, H. E. Kwak and D. Banerjee, Investigation of High Temperature Nanofluids for Solar Thermal Power Conversion and Storage Applications, 2010, *14th Int. Heat Transf. Conf. IHTC 14*, vol. 7, pp. 583–591, 2011, DOI: **10.1115/IHTC14-23296**.

6 S. Choi and J. Eastman, Enhancing thermal conductivity of fluids with nanoparticles, 1995, **https://www.osti.gov/biblio/196525**.

7 D. Shin, D. B.-I. J. of S. C. in, and undefined 2010, Effects of silica nanoparticles on enhancing the specific heat capacity of carbonate salt eutectic (work in progress), **journals.tdl.org**, vol. 2, pp. 25–31, 2010, accessed May 30, 2022, available **https://journals.tdl.org/ijscs/index.php/ijscs/article/view/2337**.

8 D. Shin and D. Banerjee, Enhanced specific heat capacity of nanomaterials synthesized by dispersing silica nanoparticles in eutectic mixtures, *J. Heat Transfer*, 2013, **135**(13), 032801, DOI: **10.1115/1.4005163**.

9 D. Shin and D. Banerjee, Specific heat of nanofluids synthesized by dispersing alumina nanoparticles in alkali salt eutectic, *Int. J. Heat Mass Transfer*, Jul. 2014, **74**, 210–214, DOI: **10.1016/j.ijheatmasstransfer.2014.02.066**.

10 S. M. M. Rizvi, B. El Far, Y. Nayfeh and D. Shin, Investigation of time–temperature dependency of heat capacity enhancement in molten salt nanofluids, *RSC Adv.*, 2020, **10**(39), 22972–22982, DOI: **10.1039/D0RA03666H**.

11 H. J. Kim and B. Jo, Anomalous Increase in Specific Heat of Binary Molten Salt-Based Graphite Nanofluids for Thermal Energy Storage, *Appl. Sci.*, 2018, **8**, 1305, DOI: **10.3390/APP8081305**.

12 B. Dudda and D. Shin, Investigation of Molten Salt Nanomaterial as Thermal Energy Storage in Concentrated Solar Power, *ASME Int. Mech. Eng. Congr. Expo. Proc.*, 2013, **9**, 813–818, DOI: **10.1115/IMECE2012-87707**.

13 M. Chieruzzi, G. F. Cerritelli, A. Miliozzi and J. M. Kenny, Effect of nanoparticles on heat capacity of nanofluids based on molten salts as PCM for thermal energy storage, *Nanoscale Res. Lett.*, 2013, **8**(1), 1–9, DOI: **10.1186/1556-276X-8-448/FIGURES/6**.

14 M. C. Lu and C. H. Huang, Specific heat capacity of molten salt-based alumina nanofluid, *Nanoscale Res. Lett.*, 2013, **8**(1), 1–7, DOI: **10.1186/1556-276X-8-292/FIGURES/5**.

15 M. Lasfargues, Q. Geng, H. Cao and Y. Ding, Mechanical Dispersion of Nanoparticles and Its Effect on the Specific Heat Capacity of Impure Binary Nitrate Salt Mixtures, *Nanomater.*, 2015, **5**(3), 1136–1146, DOI: **10.3390/NANO5031136**.

16 M. Chieruzzi, A. Miliozzi, T. Crescenzi, J. M. Kenny and L. Torre, Synthesis and Characterization of Nanofluids Useful in Concentrated Solar Power Plants Produced by New Mixing Methodologies for Large-Scale Production, *J. Heat Transfer*, 2018, **140**(4), DOI: **10.1115/1.4038415/367882**.

17 M. Chieruzzi, A. Miliozzi, T. Crescenzi, L. Torre and J. M. Kenny, A New Phase Change Material Based on Potassium Nitrate with Silica and Alumina Nanoparticles for Thermal Energy Storage, *Nanoscale Res. Lett.*, 2015, **10**(1), 1–10, DOI: **10.1186/S11671-015-0984-2/FIGURES/8**.

18 M. Chieruzzi, G. F. Cerritelli, A. Miliozzi and J. M. Kenny, Effect of nanoparticles on heat capacity of nanofluids based on molten salts as PCM for thermal energy storage, *Nanoscale Res. Lett.*, 2013, **8**(1), 1–9, DOI: **10.1186/1556-276X-8-448**.

19 M. Chieruzzi, G. F. Cerritelli, A. Miliozzi, J. M. Kenny and L. Torre, Heat capacity of nanofluids for solar energy storage produced by dispersing oxide nanoparticles in nitrate salt mixture directly at high temperature, *Sol. Energy Mater. Sol. Cells*, 2017, **167**, 60–69, DOI: **10.1016/j.solmat.2017.04.011**.

20 Z. Li, B. Li, X. Du and H. Wu, Experimental investigation on stability of thermal performances of solar salt based nanocomposite, *Renewable Energy*, 2020, **146**, 816–827, DOI: 10.1016/J.RENENE.2019.07.009.

21 N. Aslfattahi, R. Saidur, N. A. Che Sidik, M. F. Mohd Sabri and M. H. Zahir, Experimental Assessment of a Novel Eutectic Binary Molten Salt-based Hexagonal Boron Nitride Nanocomposite as a Promising PCM with Enhanced Specific Heat Capacity, *J. Adv. Res. Fluid Mech. Therm. Sci.*, 2020, **68**(1), 73–85, DOI: 10.37934/arfmts.68.1.7385.

22 E. González-Roubaud, D. Pérez-Osorio and C. Prieto, Review of commercial thermal energy storage in concentrated solar power plants: steam *vs.* molten salts, *Renewable Sustainable Energy Rev.*, 2017, **80**, 133–148, DOI: 10.1016/j.rser.2017.05.084.

23 M. X. Ho and C. Pan, Optimal concentration of alumina nanoparticles in molten Hitec salt to maximize its specific heat capacity, *Int. J. Heat Mass Transfer*, 2014, **70**, 174–184, DOI: 10.1016/J.Ijheatmasstransfer.2013.10.078.

24 C.-C. Lai, W.-C. Chang, W.-L. Hu, Z. M. Wang, M.-C. Lu and Y.-L. Chueh, A solar-thermal energy harvesting scheme: enhanced heat capacity of molten HITEC salt mixed with Sn/SiOx core–shell nanoparticles, *Nanoscale*, 2014, **6**(9), 4555, DOI: 10.1039/c3nr06810b.

25 Y. Hu, Y. He, Z. Zhang and D. Wen, Effect of Al_2O_3 nanoparticle dispersion on the specific heat capacity of a eutectic binary nitrate salt for solar power applications, *Energy Convers. Manage.*, 2017, **142**, 366–373, DOI: 10.1016/j.enconman.2017.03.062.

26 B. Dudda and D. Shin, Effect of nanoparticle dispersion on specific heat capacity of a binary nitrate salt eutectic for concentrated solar power applications, *Int. J. Therm. Sci.*, 2013, **69**, 37–42, DOI: 10.1016/j.ijthermalsci.2013.02.003.

27 M. Schuller, Q. Shao and T. Lalk, Experimental investigation of the specific heat of a nitrate-alumina nanofluid for solar thermal energy storage systems, *Int. J. Therm. Sci.*, 2015, **91**, 142–145, DOI: 10.1016/j.ijthermalsci.2015.01.012.

28 P. Andreu-Cabedo, R. Mondragon, L. Hernandez, R. Martinez-Cuenca, L. Cabedo and J. E. Julia, Increment of specific heat capacity of solar salt with SiO2 nanoparticles, *Nanoscale Res. Lett.*, 2014, **9**(1), 1–11, DOI: 10.1186/1556-276X-9-582.

29 M. Lasfargues, Q. Geng, H. Cao and Y. Ding, Mechanical dispersion of nanoparticles and its effect on the specific heat capacity of impure binary nitrate salt mixtures, *Nanomaterials*, 2015, **5**(3), 1136–1146, DOI: 10.3390/nano5031136.

30 N. Navarrete, L. Hernández, A. Vela and R. Mondragón, Influence of the production method on the thermophysical properties of high temperature molten salt-based nanofluids, *J. Mol. Liq.*, 2020, **302**, 112570, DOI: 10.1016/j.molliq.2020.112570.

31 U. Nithiyanantham, L. González-Fernández, Y. Grosu, A. Zaki, J. M. Igartua and A. Faik, Shape effect of Al_2O_3 nanoparticles on the thermophysical properties and viscosity of molten salt nanofluids for TES application at CSP plants, *Appl. Therm. Eng.*, 2020, **169**, 114942, DOI: 10.1016/j.applthermaleng.2020.114942.

32 Z. Yinping, J. Yi and J. Yi, A simple method, the history method, of determining the heat of fusion, specific heat and thermal conductivity of phase-change materials, *Meas. Sci. Technol.*, 1999, **10**(3), 201–205, DOI: 10.1088/0957-0233/10/3/015.

33 D. Ranjan Parida, N. Dani and S. Basu, Data-driven analysis of molten-salt nanofluids for specific heat enhancement using unsupervised machine learning methodologies, *Sol. Energy*, 2021, **227**, 447–456, DOI: 10.1016/J.SOLENER.2021.09.022.

34 Sigma-Aldrich, TEM image of aluminum oxide (544833), https://www.sigmaaldrich.com/deepweb/content/dam/sigma-aldrich/product2/056/e033342.jpg/_jcr_content/renditions/e033342-large.jpg.

35 C. Y. Tang, Q. Shiang Fu, D. Gao, C. S. Criddle and J. O. Leckie, Effect of solution chemistry on the adsorption of perfluorooctane sulfonate onto mineral surfaces, *Water Res.*, 2010, **44**(8), 2654–2662, DOI: 10.1016/J.WATRES.2010.01.038.

36 F. Inam, H. Yan, T. Peijs and M. J. Reece, The sintering and grain growth behaviour of ceramic–carbon nanotube nanocomposites, *Compos. Sci. Technol.*, Jun. 2010, **70**(6), 947–952, DOI: 10.1016/j.compscitech.2010.02.010.

37 M. Toledo, *Thermal Analysis UserCom*, 7, 1998, available https://www.mt.com/us/en/home/library/usercoms/lab-analytical-instruments/thermal-analysis-usercom-7.html.

38 ASTM International, *E1269-11 Standard Test Method for Determining Specific Heat Capacity by Differential Scanning Calorimetry*, ASTM Int., 2011, doi: DOI: 10.1520/E1269-11.

39 T. L. Bergman, F. P. Incropera, D. P. DeWitt and A. S. Lavine, *Fundamentals of heat and mass transfer*, John Wiley & Sons, 2011.

40 A. J. N. Khalifa, Natural convective heat transfer coefficient – a review: I. Isolated vertical and horizontal surfaces, *Energy Convers. Manag.*, 2001, **42**(4), 491–504, DOI: 10.1016/S0196-8904(00)00042-X.

41 A. J. N. Khalifa, Natural convective heat transfer coefficient – a review: II. Surfaces in two- and three-dimensional enc`losures, *Energy Convers. Manage.*, 2001, **42**(4), 505–517, DOI: 10.1016/S0196-8904(00)00043-1.

42 M. X. Ho and C. Pan, Experimental investigation of heat transfer performance of molten HITEC salt flow with alumina nanoparticles, *Int. J. Heat Mass Transfer*, 2017, **107**, 1094–1103, DOI: 10.1016/j.ijheatmasstransfer.2016.11.015.

43 B. Ma, D. Shin and D. Banerjee, Synthesis and Characterization of Molten Salt Nanofluids for Thermal Energy Storage Application in Concentrated Solar Power Plants—Mechanistic Understanding of Specific Heat Capacity Enhancement, *Nanomater.*, 2020, **10**(11), 2266, DOI: 10.3390/NANO10112266.

44 A. Solé, L. Miró, C. Barreneche, I. Martorell and L. F. Cabeza, Review of the T-history method to determine thermophysical properties of phase change materials (PCM), *Renewable*

Sustainable Energy Rev., 2013, **26**, 425–436, DOI: 10.1016/J.RSER.2013.05.066.

45 E. D. Kravvaritis, K. A. Antonopoulos and C. Tzivanidis, Experimental determination of the effective thermal capacity function and other thermal properties for various phase change materials using the thermal delay method, *Appl. Energy*, 2011, **88**(12), 4459–4469, DOI: 10.1016/J.APENERGY.2011.05.032.

46 A. Caraballo, S. Galán-Casado, Á. Caballero and S. Serena, Molten salts for sensible thermal energy storage: a review and an energy performance analysis, *Energies*, 2021, **14**(4), 1197, DOI: 10.3390/en14041197.

47 M. D. Silverman and J. R. Engel, *Survey of technology for storage of thermal energy in heat transfer salt*, 1977.

48 Y. T. Wu, C. Chen, B. Liu and C. F. Ma, Investigation on forced convective heat transfer of molten salts in circular tubes, *Int. Commun. Heat Mass Transfer*, 2012, **39**(10), 1550–1555, DOI: 10.1016/j.icheatmasstransfer.2012.09.002.

49 A. G. Fernández, H. Galleguillos, E. Fuentealba and F. J. Pérez, Thermal characterization of HITEC molten salt for energy storage in solar linear concentrated technology, *J. Therm. Anal. Calorim.*, 2015, **122**(1), 3–9, DOI: 10.1007/s10973-015-4715-9.

50 Y. T. Wu, Y. Li, N. Ren, R. P. Zhi and C. F. Ma, Experimental study on the thermal stability of a new molten salt with low melting point for thermal energy storage applications, *Sol. Energy Mater. Sol. Cells*, 2018, **176**, 181–189, DOI: 10.1016/J.SOLMAT.2017.12.001.

51 G. J. Janz and G. N. Truong, Melting and Premelting Properties of the $KN0_3$-$NaN0_2$-$NaN0_3$ Eutectic System, *J. Chem. Eng. Data*, 1983, **28**(2), 201–202, DOI: 10.1021/je00032a022.

52 P. Zhang, J. Cheng, Y. Jin and X. An, Evaluation of thermal physical properties of molten nitrate salts with low melting temperature, *Sol. Energy Mater. Sol. Cells*, 2018, **176**, 36–41, DOI: 10.1016/j.solmat.2017.11.011.

53 P. E. McKnight and J. Najab, Mann-Whitney *U* test, *Corsini Encycl. Psychol.*, pp. 1, Jan. 2010, DOI: 10.1002/9780470479216.CORPSY0524.

54 T. W. MacFarland and J. M. Yates, Mann–Whitney *U* test, *Introd. to Nonparametric Stat. Biol. Sci. Using R*, 2016, pp. 103–132, DOI: 10.1007/978-3-319-30634-6_4.

55 G. W. Corder and D. I. Foreman, *Nonparametric Statistics for Non-Statisticians: A Step-by-Step Approach*, John Wiley & Sons, Inc., 2011.

56 D. Shin and D. Banerjee, Enhanced specific heat of silica nanofluid, *J. Heat Transfer*, 2011, **133**(2), DOI: 10.1115/1.4002600/467874.

57 L. Sang and T. Liu, The enhanced specific heat capacity of ternary carbonates nanofluids with different nanoparticles, *Sol. Energy Mater. Sol. Cells*, 2017, **169**, 297–303, DOI: 10.1016/J.SOLMAT.2017.05.032.